



Hydro-chemo-mechanical coupling in sediments: Localized mineral dissolution



Minsu Cha^{a,*}, J. Carlos Santamarina^b

^a Department of Civil Engineering, Texas A&M University, 3136 TAMU, College Station, TX 77843-3136, USA

^b Earth Science and Engineering, King Abdullah University of Science and Technology (KAUST), Thuwal 23955-6900, Saudi Arabia

HIGHLIGHTS

- The paper studies localized dissolution in noncohesive soils under effective stress.
- Sediments become more compressible after localized dissolution.
- The porosity increases within pipes, filled with loose non-soluble quartz.
- Shear wave velocity decreases, and codas indicate increased spatial variability.
- Principal stress rotates in pipes, and sediment reaches Coulomb failure condition.

ARTICLE INFO

Article history:

Received 27 December 2015

Received in revised form 1 March 2016

Accepted 3 June 2016

Available online 11 June 2016

Keywords:

Mineral dissolution

One-dimensional flow test

Reactive flow

Discrete element method

Localized dissolution

Hydro-chemo-mechanical coupling

ABSTRACT

Mineral dissolution is inherently a chemo-hydro-mechanical coupled process. Field evidence and laboratory results show that dissolution may localize and form open conduits in cohesive media such as carbonate rocks. This study focuses on the evolution of localized dissolution in soils (i.e., frictional and non-cohesive granular materials) under effective confining stresses. Experimental results show the development of localized dissolution (“pipe”) when a carbonate-quartz sand is subjected to reactive fluid flow: only loosely packed quartz grains remain within pipes, and the number of pipes decreases away from the inlet port. Concurrent shear wave velocity measurements show a decrease in stiffness during dissolution due to stress and fabric changes, and more complex signal codas anticipate the development of internal heterogeneity. The discrete element method is used to simulate localized vertical dissolution features in granular materials, under constant vertical stress and zero lateral strain far-field boundaries. As porosity increases along dissolution pipes, vertical load is transferred to the surrounding soils and marked force chains develop. In terms of equivalent stress, principal stress rotation takes place within pipes and the sediment reaches the Coulomb failure condition inside pipes and in the surrounding medium. Dissolution pipes alter the geo-plumbing of the subsurface, enhance fluid transport but limit the long term performance of storage systems, alter the fluid pressure and effective stress fields, soften the sediment and may trigger shear failures.

© 2016 Elsevier Ltd. All rights reserved.

1. Introduction

Mineral dissolution and re-precipitation are common processes in the chemical weathering of soils and rocks, and typically involve changes in mineralogy towards more stable compositions within a given geologic environment.

* Corresponding author.

E-mail addresses: mcha@tamu.edu (M. Cha), Carlos.Santamarina@kaust.edu.sa (J.C. Santamarina).

<http://dx.doi.org/10.1016/j.gete.2016.06.001>

2352-3808/© 2016 Elsevier Ltd. All rights reserved.

List of symbols and abbreviations

D	Chemical diffusion coefficient (m^2/s)
D_{10}	Grain diameter (in mm) corresponding to the 10% percentile by weight
D_{50}	Grain diameter (in mm) corresponding to the 50% percentile by weight
Da	Damköhler number
g	Gravitational acceleration
h	Representative vertical length scale
HR	Percentage of rotationally hindered particles in a specimen
i	Hydraulic gradient
ID	Inner diameter
k_0	Coefficient of at-rest lateral earth pressure
k_a	Coefficient of active and passive lateral earth pressure
l	Characteristic length scale of the problem (m)
n	Porosity
Pe	Péclet number
Ri	Richardson number
SF	Fraction of soluble particles
v	Flow velocity (m/s)
V_s	Shear wave velocity
α	Shear wave velocity at $\sigma' = 1$ kPa
β	Stress sensitivity of the shear wave velocity
ε_h	Lateral strain conditions
ϕ	Sediment angle of internal shear strength
θ	Reaction rate constant (1/s)
σ	Effective stress (σ_1 and σ_+ direction of propagation and particle motion; σ_1 and σ_3 minor and major principal stress)

Layering and discontinuities, state of stress, changes in fluid chemistry and gravity-dominated fluid flow contribute to the development of preferential flow paths in sediments and rocks.^{1–3} Vertical tubes are initiated by infiltration, while horizontal tubular cavities result from strata bound water flow.⁴ Dissolution is relatively slow in nature, yet, geological strata that contain carbonates or evaporites are particularly prone to dissolution in high fluid advection systems. Localized dissolution is the cause of sinkholes and settlements in karst regions and calcareous terrains.⁵

Human activity can move natural systems far from equilibrium, such as the injection fluids that change the natural pH and pumping-driven advective transport.^{6,7} Accelerated dissolution rates caused by high hydraulic gradients undermine the performance of dams by increasing uplift pressure and accelerating seepage and piping.^{8–10} The dissociation of load-bearing gas hydrate leads to instability in sediments and has been considered the cause of marine landslides.^{11–14} The geological storage of CO_2 acidifies pore water and causes mineral dissolution that may lead to porosity and mineralogy changes, settlement, and tensile fracturing of the seal rock.^{15–20} Dissolution and precipitation affects permeability changes over time in enhanced geothermal systems.^{21,22} Finally, the consequences of dissolution extend beyond geosystems; for example,

dissolution is one of the main causes of natural deterioration of Portland cement concrete by acid rain,^{23,24} and demineralization makes bones porous and vulnerable to brittle fractures.²⁵

Chemical reaction, advective mass transport, and diffusive transport rates control the evolving topology of dissolution. These can be captured in two dimensionless numbers in terms of flow velocity v (m/s), the characteristic length scale of the problem l (m), the chemical diffusion coefficient D (m^2/s), and the reaction rate constant θ (1/s):

$$\text{Péclet number } Pe = \frac{vl}{D} = \frac{\text{Advective transport rate}}{\text{Diffusive transport rate}} \quad (1)$$

$$\text{Damköhler number } Da = \frac{\theta l}{v} = \frac{\text{Reaction rate}}{\text{Advective transport rate}} \quad (2)$$

Experimental and numerical studies show dissolution topology in terms of Pe and Da numbers:^{26–28} (a) compact dissolution when $Pe < 10^{-3}$, (b) uniform dissolution when $Da < 10^{-3}$, (c) dissolution localization at high $Da > 10^{-2}$ and $Pe > 10^{-2}$ numbers. In addition, density variation in the fluid affects dissolution morphologies due to gravity;²⁹ buoyancy prevails over advection when the Richardson number $Ri = gh/v^2 \geq 1$, where g is the gravitational acceleration and h is a representative vertical length scale.³⁰

Previous studies reveal that homogeneously distributed particle-scale dissolution affects both the small and large-strain properties of sediments:^{31–34} a distinct “honeycomb fabric” emerges,³⁵ vertical displacement and void ratio increase,^{36,33,37–39} the stress ratio between horizontal to vertical effective stress k_0 decreases often to Rankine- k_a failure condition,³⁷ shear wave velocity decreases and attenuation increases,^{33,36} and the peak friction angle decreases.³⁶ Furthermore, fluid permeability changes,⁴⁰ and strain localization may emerge.³⁵ Hu and Hueckel (2007)⁴¹ and Pietruszczak et al. (2006)⁴² introduced important concepts and models of chemo-mechanical couplings for granular contact dissolution and deformation.

This study centers on coupled chemo-hydro-mechanical processes during dissolution in uncemented granular materials under effective confining stress. First, experimental evidence is presented for the emergence of localized dissolution in sediments. Then, discrete element numerical simulations are conducted to gain particle-level insight on the mechanical consequences of localized dissolution in soils.

2. Experimental study

Device and materials. The experimental study is conducted using a quartzitic-carbonate sandy sediment from the Atlantic coastal plains in Georgia, USA ($D_{10} = 0.25$ mm; $D_{50} = 0.8$ mm; 100% passes sieve #10 and is retained on sieve #100. Composition: 52% calcite, 47% quartz, and trace of clay minerals). The chamber is a zero-lateral strain cell (stainless steel cell, ID = 100 mm— Fig. 1); the lower and upper loading plates have a dense groove pattern beneath porous stones to ensure even 1D flow. A linear variable differential transducer LVDT attached to the

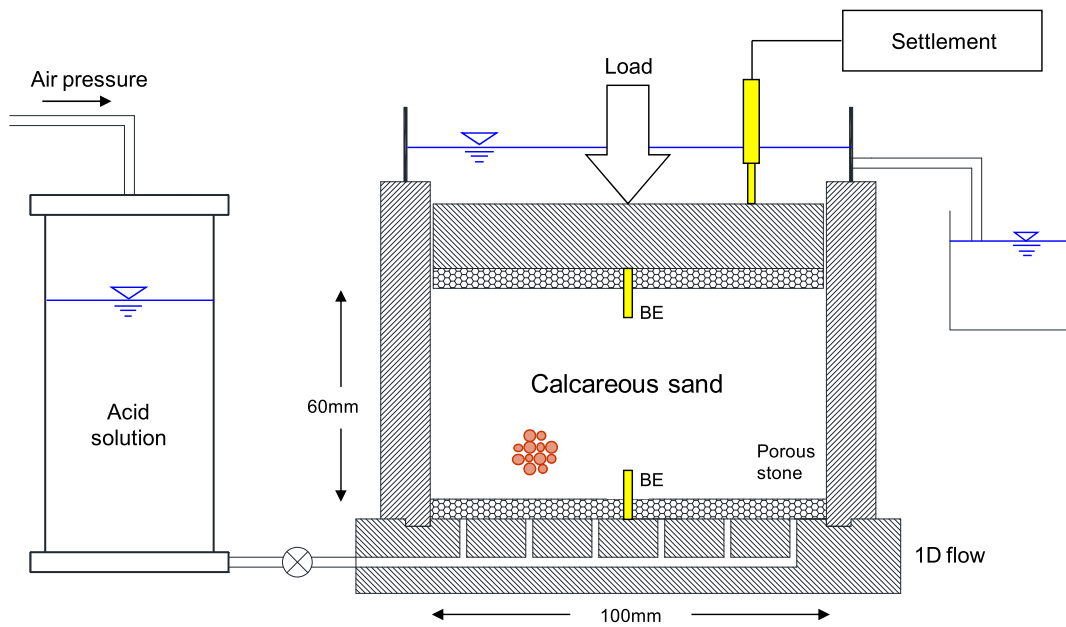


Fig. 1. Experimental study of dissolution in a zero-lateral strain cell. 1D flow is enforced at constant inlet fluid pressure. Note: piezocrystal bender elements BE are used for shear wave generation and detection.

loading plates tracks the sediment vertical displacement. Piezo-ceramic bender elements installed at the bottom and top plates are used to monitor the evolution of shear wave velocity in the sediment throughout the experiment. Fluid flow is imposed through the bottom plate.

Procedure. The dry sediment is prepared in a zero-lateral strain cell (stainless steel cell, ID = 100 mm; 60 mm sediment height— Fig. 1), and then loaded in several steps to 200 kPa vertical stress. While subjecting the sediment to a constant 200 kPa vertical stress: (1) 9 liters (~ 20 pore volumes) of tap water are passed through the sediment to saturate it; (2) a slight settlement observed during and after the water flow due to soil wetting is fully stabilized and the sediment is allowed to chemically equilibrate with the introduced pore water for 72 h; (3) 12 liters (~ 25 pore volumes) of 1 molar solution of acetic acid CH_3COOH are injected through the bottom porous stone at a constant hydraulic gradient ($i = 35$) while effluent is collected from the top cap; then, (4) fresh water is flushed through the sediment to stop chemical reactions. Finally, the sediment is further loaded 900 kPa vertical effective stress to compare the pre and post dissolution compressibilities. After unloading, the specimen is carefully extruded from the cell, and subjected to tomographic imaging, followed by slicing for visual inspection and mineral analysis.

Results. Load-dissolution tests were repeated with various specimens subjected to different vertical effective stress levels ($\sigma_z = 200$ and 400 kPa), flow rates, and molar concentrations of acetic acid.

Specimens settle almost linearly with time during reactive fluid flow until fresh water is flushed through the sediment to remove acid (Fig. 2). Void ratio is calculated using recorded vertical deformation (thus volume) and measuring dry soil weight before and after dissolution tests. Specimens also settle almost linearly with the log of the applied

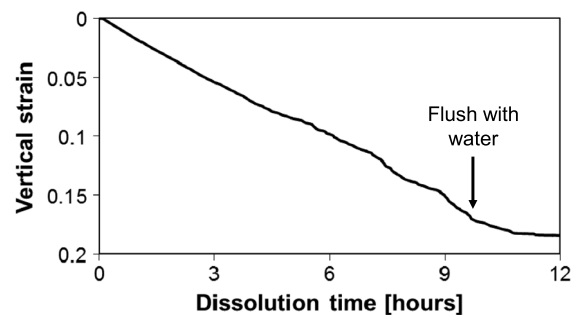


Fig. 2. Vertical strain vs. time during the reactive flow.

vertical stress during loading (Fig. 3). The volume-average global void ratio increases during dissolution (from $e = 0.64$ to $e = 0.75$ for the case reported in Fig. 3). The sediment compressibility $\Delta e / \log[(\sigma + \Delta\sigma)/\sigma]$ is higher after dissolution than before dissolution (almost doubled in Fig. 3), and the post-dissolution sediment has an increased tendency to volumetric contraction upon loading.

The shear wave velocity experienced a pronounced drop during dissolution even though the effective stress remained constant (Fig. 3). Signature codas gained marked complexity during dissolution (not shown), anticipating the increased spatial variability evolving inside the specimen.

Tomographic images reveal the presence of distinct low-density vertical columns; the localized dissolution structure is confirmed by gradually shaving sediment layers from the top, as shown in Fig. 4 where dark brown regions show the volume affected by dissolution surrounded by the light colored natural sediment. We will call this low-density regions resulted from localized dissolution as “pipe” to highlight its function as a high-permeability path. In the similar context, “wormholes” are

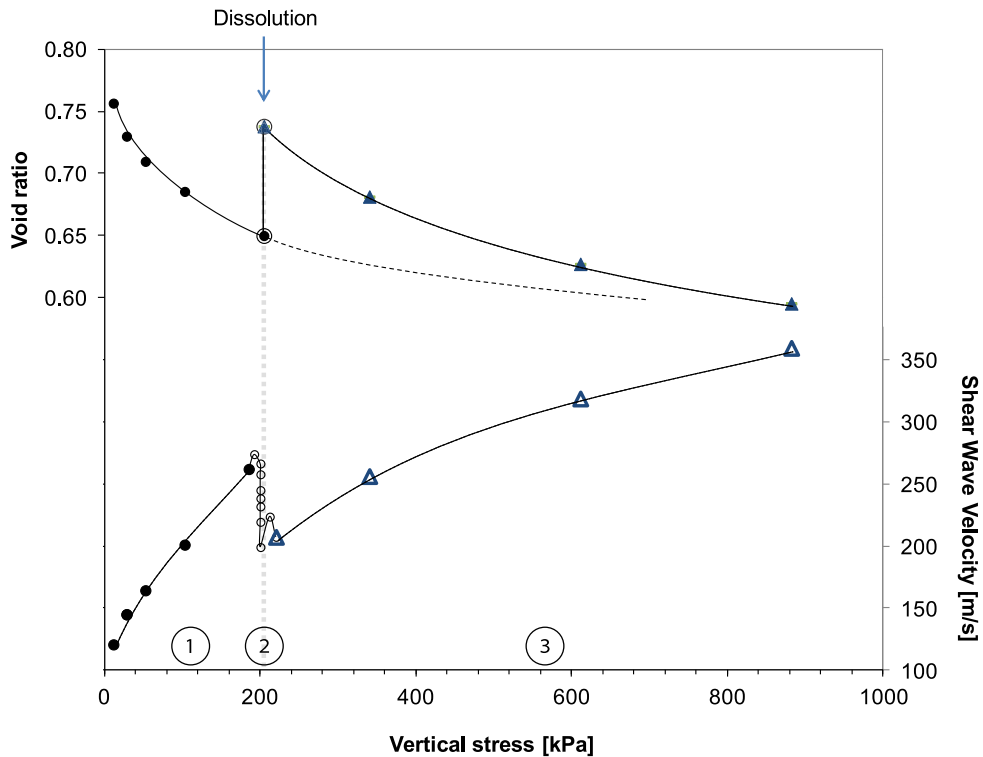


Fig. 3. Void ratio and shear wave velocity changes during ① loading, ② reactive fluid transport and dissolution, and ③ additional loading. Device shown in Fig. 1.

used for dissolution cavities created in carbonate rocks.^{26,27} Unlike complete voids in wormholes, pipes in our study are filled with insoluble or less soluble grains such as quartz. XRD results show that the mineralogy of the background medium consists of both quartz and calcite, but that only quartz remains in pipes i.e., there has been a ~52% mass loss in pipes (Fig. 4). Calcite has been completely dissolved at the inlet surface due to its direct contact with acid solution; some pipes are fully formed from inlet to outlet, while others appear as abandoned pathways. From volumetric analyses and X-ray intensity, the internal porosity in pipes is estimated to be $n = 0.47$.

3. Discrete element simulation

Discrete element simulations represent the sediment as an arrangement of individual particles in a Newtonian mechanics framework.⁴³ The discrete element code PFC (ITASCA Consulting Group, Inc.) is used to study the geomechanical implications of localized dissolution both in 2D and 3D conditions in order to gain particle-scale insight during localized dissolution. The simulation environment is summarized in Table 1. The interparticle friction coefficient is 0.5, and there is no friction between grain and the rigid lateral boundaries (i.e., zero-lateral strain conditions $\varepsilon_h = 0$). In both 2D and 3D cases, the granular packing is formed by randomly placing small grains with uniform size distribution in a container and gradually expanding them under zero gravity and zero interparticle

friction to attain the target porosity (similar approach to Refs. [44,45]). The gradual expansion process involves a re-equilibrium stage before attempting the next expansion step; more than 5000 expansion-equilibration cycles are conducted to form the granular packing.

Grain angularity implies rotational resistance and it is simulated by hindering the rotation of a fraction of randomly selected grains (Percentage of particles with hindered rotation in a specimen $HR = 0\%$ for “round particles” and 80% for “angular particles”). The vertical stress is kept constant during dissolution using a numerical servo-control function. The positions and sizes of vertical columnar regions that will undergo dissolution, and insoluble regions (“host”) are predefined in the sediment, and soluble particles (in red) are chosen at random (Table 1). The fraction of soluble particles within the columns are $SF = 25\%$ and 50% in 2D, and $SF = 50\%$ and 100% in 3D simulations. Dissolution is simulated by gradually decreasing the size of all the soluble particles over time at the same rate. The gradual size reduction involves numerous steps of minute size reduction (radius reduction of $1/50\,000$ times initial radius in each step), each step followed by a full equilibrium stage. In particular, the ratio of the mean unbalanced force to the mean contact force is always smaller than 0.001 to ensure stable conditions throughout the dissolution processes. The results subset presented next adequately represents all trends observed in this study (complete results in Ref. [46]).

Normalized vertical displacement (Fig. 5(a)). While dissolution takes place in soluble columns only, sediments

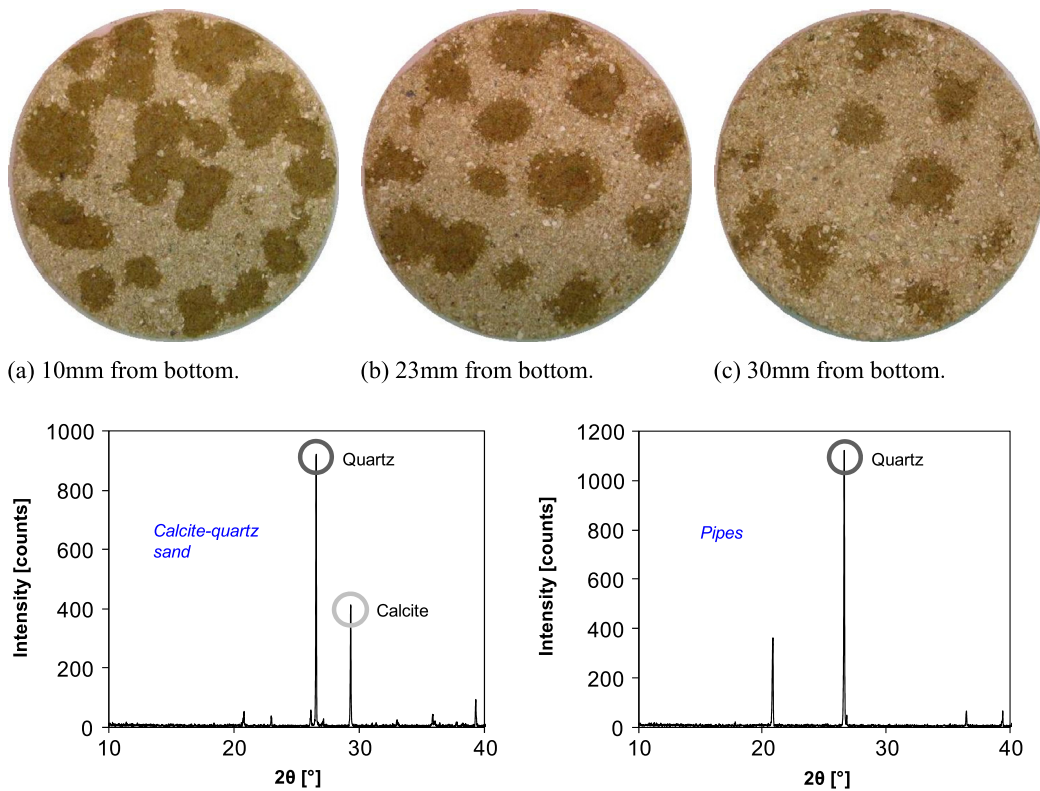


Fig. 4. Specimen dissection by successive layer removal. Slices at various depths show localized carbonate dissolution. The light-color sand has both carbonate and quartz; the dark-color sand patches are the carbonate-free pipes after dissolution. Mineral composition: XRD spectra correspond to the carbonate-quartz around pipes, and the non-soluble quartz grains that remain in pipes. (For interpretation of the references to color in this figure legend, the reader is referred to the web version of this article.)

settle almost linearly with the mass loss of soluble grains SF during early stages of dissolution (the mass loss is captured using the normalized size reduction $\Delta R/R_0$ —similar response was experimentally observed). Angular sediments HR = 80% experience lower vertical displacement particularly in 3D simulations due to higher interlocking and rotational frustration that hinders particle rearrangement.

Porosity (Fig. 5(b)). Porosity increases within dissolved regions (pipes) and to a lesser extent in the surrounding medium. Interlocked sediments with hindered rotation (HR = 80%) experience a higher increase in porosity. Sudden collapse events in angular interlocked sediments are accompanied by changes in porosity.

Equivalent global stress ratio $k_0 = \sigma_h/\sigma_v$ (Fig. 5(c)). Equivalent stresses can be readily computed from inter-particle forces and affected areas. The equivalent horizontal stress σ_h acting against the boundaries in both 2D and 3D systems increases in sediments with no interlocking (HR = 0%) during early stages of dissolution, but it decreases in interlocked sediments (HR = 80%). Similar trends have been numerically and experimentally observed when dissolving grains are homogeneously distributed throughout the sediment.^{31,37}

Contact force chains. Force chains are strong in the vertical direction before dissolution, in agreement with principal stress directions. After dissolution, marked force

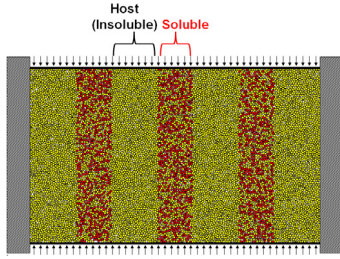
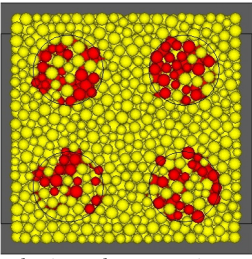
chains remain preferentially vertical away from pipes, yet, they are preferentially horizontal within pipes (Fig. 6). In fact, horizontal contact forces inside pipes prevent the buckling of granular columns in the surrounding sediment. As dissolution continues, surrounding soils slide towards the looser pipes, and structural differences between the two zones become less prominent (Fig. 6(c)).

4. Discussion and implications

Experiments and simulations were designed to gather complementary information. General trends clearly show strong parallels between experimental and numerical results, in particular, linear settlement with the progression of dissolution and increased porosity in pipes and global (experiment: $n = 0.39$ to 0.43 ; 3D numerical: $n = 0.40$ to 0.43 for HR = 0% and $n = 0.40$ to 0.48 for HR = 80%). Innate differences between numerical and experimental conditions hinder further quantitative comparisons, due to bottom-up vs. simultaneous dissolution, random vs. predetermined pipe location, natural grains vs. spherical particles with hindered rotation.

The analysis of particle-scale forces in terms of equivalent stresses can be extended to explore the interaction between grains in pipes and in the surrounding host medium. The equivalent vertical stress increases rapidly

Table 1
DEM simulation environment.

Properties	2D	3D
Configurations—insoluble (“host”) and soluble regions		
Particle properties		
Particle size distribution	Uniform size distribution ($R_{\min} = 0.3 \text{ mm}$, $R_{\max} = 0.45 \text{ mm}$)	Uniform size distribution ($R_{\min} = 1 \text{ mm}$, $R_{\max} = 1.5 \text{ mm}$)
Number of particles	11 272 disks	9167 spheres
Particle density	2650 kg/m ³	2650 kg/m ³
Contact model	Linear contact model – Normal stiffness $k_n = 10^8 \text{ N/m}$ – Shear stiffness $k_s = 10^8 \text{ N/m}$	Hertzian contact model – Shear modulus = $2.9 \times 10^9 \text{ Pa}$ – Poisson's ratio = 0.3
Inter-particle friction	0.5	0.5
Hindered rotation HR	0% and 80%	0% and 80%
Fraction of soluble particles in predefined soluble regions SF	25% and 50% (red particles in the configuration above)	50% and 100% (red particles in the configuration above)
Boundary conditions		
Initial cell size	(Height × Width) 6 cm × 10 cm	(Height × Width × Length) 5 cm × 5 cm × 5 cm
Vertical load	100 kPa (during dissolution)	100 kPa (during dissolution)
Lateral boundaries	Zero strain	Zero strain
Particle-to-wall friction	0	0

in the host medium when dissolution starts in pipes, as vertical load is shed to the host medium (Fig. 7—Note: global vertical equilibrium with boundary loads is verified in all cases). In the horizontal direction, horizontal stresses σ_h in pipes and host are almost identical $\sigma_{h|_{\text{pipe}}} \approx \sigma_{h|_{\text{host}}}$, in agreement with equilibrium requirements. Principal stresses rotate inside pipes during dissolution as the vertical stress decreases and the horizontal stress increases to become the major principal stress. The peak equivalent global stress ratio $\sigma_1/\sigma_3|_{\text{max}}$ reaches the Coulomb failure condition $\sigma_1/\sigma_3 = \tan^2(45 - \phi/2)$ both in the pipes and in the host medium.

The shear wave velocity V_s followed a Hertzian power-type trend during loading, both before and after dissolution (Fig. 3). In uncemented granular materials, the shear wave velocity is determined by the mean stress in the polarization, i.e., the average between the stress in the direction of propagation σ_1 and in the direction of particle motion σ_+

$$V_s = \alpha \left(\frac{\sigma_1 + \sigma_+}{2 \text{ kPa}} \right)^\beta. \quad (3)$$

Fitted parameters before ($\alpha = 74 \text{ m/s}$, $\beta = 0.226$) and after dissolution ($\alpha = 28 \text{ m/s}$, $\beta = 0.394$) show higher stiffness sensitivity to stress after dissolution. This is in agreement with the higher sediment compressibility after dissolution observed in experimental results (Fig. 3), i.e., there is a rapid increase in coordination number when loosely packed grains are subjected to loading. These results fall in with data compiled for loose and densely packed natural soils worldwide.⁴⁷ The shear wave velocity

dropped from 274 m/s to 199 m/s during dissolution at constant vertical effective stress σ_1 (Fig. 3). Given that the horizontal stress cannot be smaller than the condition at Coulomb failure, $\sigma_+ \geq \sigma_1 \tan^2(45 - \phi/2)$, this marked decrease in velocity cannot be justified by a decrease in transverse stress σ_+ alone Eq. (3). Hence, shear-wave velocity tracks changes in stiffness due to the applied stress and due to fabric changes associated with dissolution.

The highly porous flow paths created by localized dissolution alters the “geo-plumbing” of the subsurface by creating highly permeable conduits underground that facilitate flow. These hydraulic short-circuit paths can be engineered to enhance fluid transport (e.g., acid treatment for enhanced oil recovery); however, their emergence often diminishes system efficiency (e.g., enhanced geothermal systems), or limit the long term performance of storage systems (e.g., dams and CO₂ geological storage). Furthermore, localized dissolution pipes bring high fluid pressure fronts towards the outlet, increase the hydraulic uplift pressure, heighten the vulnerability to retrogressive piping erosion, lower the effective stress in the medium, and systems subjected to shear may experience failure (e.g., slopes).

The nucleation of localized dissolution in rocks is often associated to the presence of high conductivity natural fractures or interlayers with hydraulic conductivity contrast. Dissolution evolves as a consequence of gravity, convection and advection and creates open cavities and conduits. Karst topology is a salient example.

In contrast, dissolution pipes in soils emerge as a consequence of the spatially-correlated pore size variability in natural sediments whereby most of the flow takes

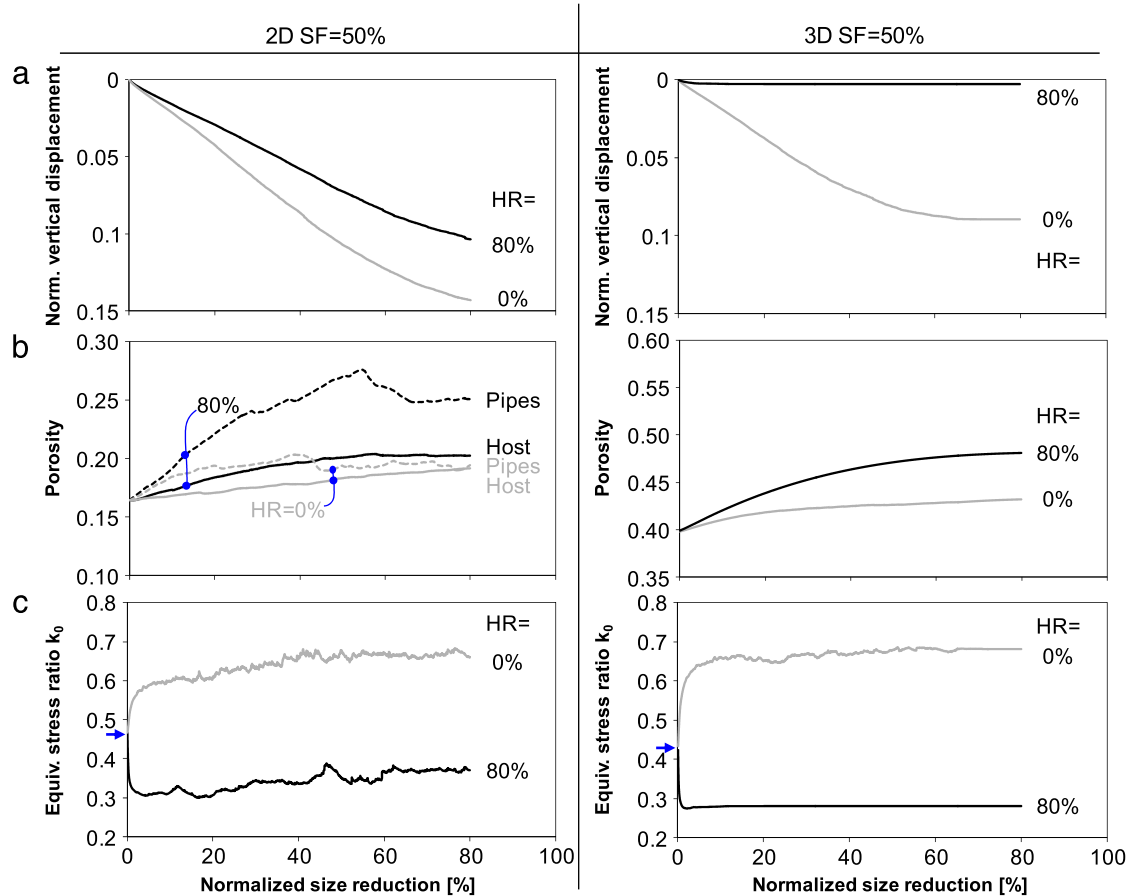


Fig. 5. Sediment response during localized dissolution under zero lateral strain. 2D and 3D numerical simulations (a) Normalized vertical displacement. (b) Porosity. (c) Equivalent global stress ratio $k = \sigma_h/\sigma_v$. Note: grains in the “host” medium experience no dissolution while SF = 50% of grains in pipes dissolve. Simulation details in Table 1.

place through a small fraction of the pore space.⁴⁸ Under these conditions, reactive fluid transport creates the positive feedback conditions to favor dissolution along the already more previous paths. However, open cavities cannot form in uncemented sediments, and neighboring sediments continue yielding into dissolving channels until they are filled with loosely packed insoluble grains. Therefore, the formation of dissolution pipes in soils is inherently a coupled hydro-chemo-mechanical phenomenon.

The modified pressure and flow fields around a pipe hinder the formation of other pipes nearby. The exclusion distance decreases and the pipe density increases with increasing flow rate.^{49,27} Longer pipes reach closer to the outlet, have higher exit gradients, transport more fluid, grow faster than smaller ones, and there is a lower pipe density towards the outlet⁵⁰ as observed in Fig. 4.

5. Conclusions

Hydro-chemo-mechanical coupling can lead to dissolution localization in single- and multi-mineral sediments. The number of dissolution pipes decreases away from the inlet port. While porosity increases within pipes, empty cavities cannot form in cohesionless sediments. The

sediments that have undergone localized dissolution are more compressible than pre-dissolution sediments.

Marked force chains form within pipes and in the surrounding medium as a result of internal unloading and pronounced force redistribution during dissolution. In terms of equivalent stresses, principal stress may rotate inside pipes, and the stress ratio may reach the Coulomb failure condition both in pipes and in the host medium.

Concurrent geophysical monitoring using shear-wave propagation reflects undergoing changes in stiffness due to both changes in effective stress (Hertzian effect) and fabric evolution during dissolution. More complex signal codas reveal the development of internal heterogeneity.

Dissolution pipes alter the geo-plumbing of the subsurface, enhance fluid transport but limit the long term performance of storage systems, alter the fluid pressure and effective stress fields, soften the sediment and may cause shear failure.

Acknowledgments

Support for this research was provided by the Department of Energy Savannah River Operations Office led by Dr. B. Gutierrez. Additional support was provided by

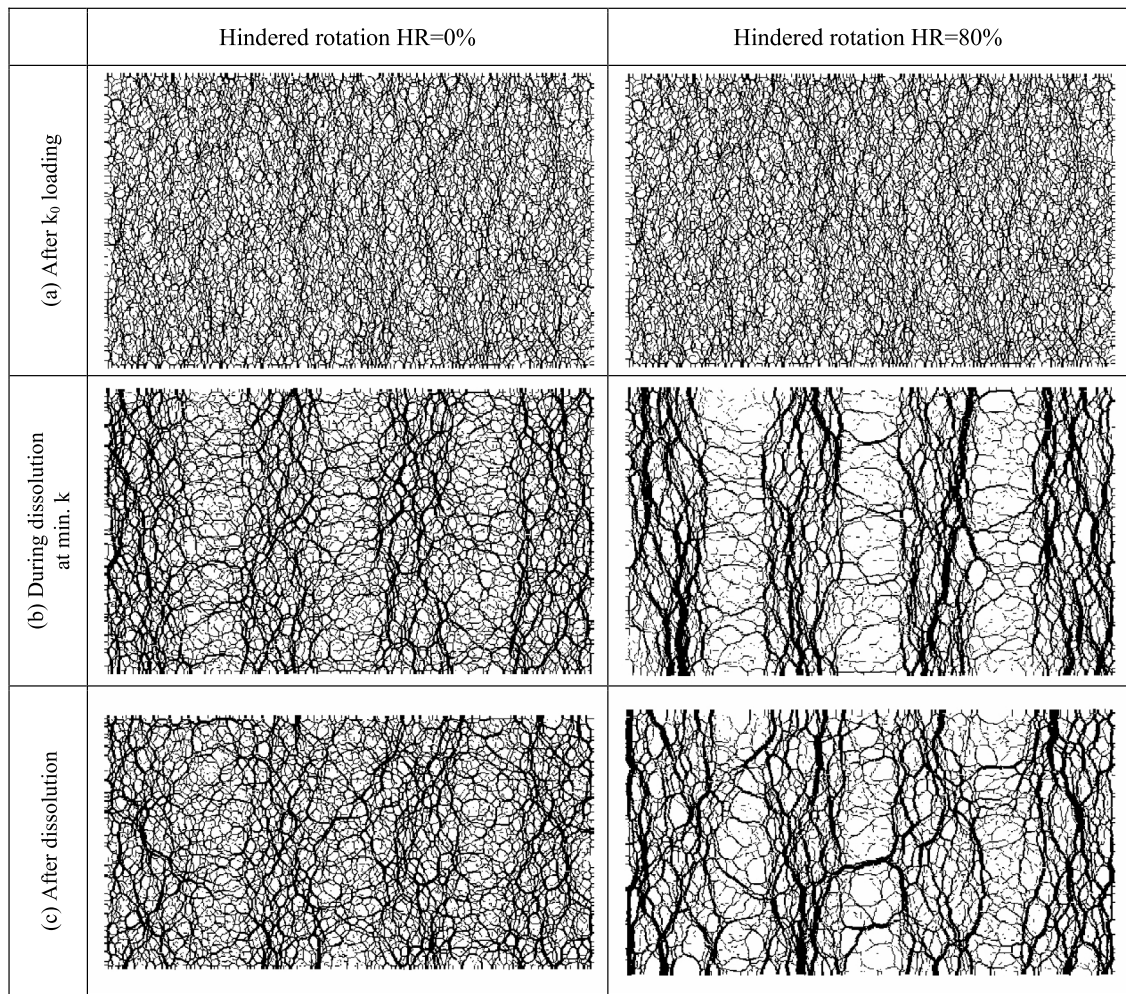


Fig. 6. Evolution of contact force chains during localized dissolution along pipes (2D and SF = 50% within the pipes). (a) After zero lateral strain loading and before dissolution. (b) During dissolution at minimum stress ratio $k = \sigma_h/\sigma_v$. (c) After complete dissolution. Note: The network of contact lines is drawn with thickness proportional to normal contact forces. Simulation details in Table 1.

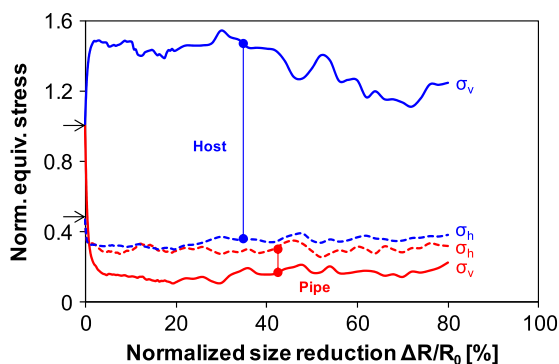


Fig. 7. Evolution of the equivalent horizontal σ_h and vertical σ_v stresses normalized by the constant vertical stress applied during dissolution. Trends shown for sediments in pipes and in the host medium (Note: 2D simulation; SF = 50% within the pipes; hindered rotation HR = 80%). Simulation details in Table 1.

the Goizueta Foundation. The authors are grateful to the anonymous reviewers for their valuable comments.

References

- [1] Boggus M, Crawford R. Explicit Generation of 3D Models of Solution Caves for Virtual Environments. In: *Proceedings of the 2009 International Conference on Computer Graphics and Virtual Reality* 2009.
- [2] Criss EM, Criss RE, Osburn GR. Effects of stress on cave passage shape in karst terranes. *Rock Mech Rock Eng.* 2008;41(3):499–505.
- [3] Gillieson DS. *Caves: Processes, Development, and Management*. Oxford: Blackwell Publishers; 1996.
- [4] Ford D, Williams PW. *Karst Hydrogeology and Geomorphology*. Chichester, West Sussex, England: Wiley; 2007.
- [5] Waltham T. *Foundations of Engineering Geology*. third ed. New York, NY: Spon Press; 2009: edn.
- [6] Hunt RE. *Geologic Hazards: A Field Guide for Geotechnical Engineers*. Boca Raton, USA: CRC Press; 2007.
- [7] Veni G, Duchene H, Crawford NC, Groves CG, Huppert GN, Kastning EH, Olson R, Wheeler BJ. *Living With Karst: A Fragile Foundation*. American Geological Institute; 2001.
- [8] Gutiérrez F, Desir G, Gutiérrez M. Causes of the catastrophic failure of an earth dam built on gypsiferous alluvium and dispersive clays (Altorción, Huesca Province, NE Spain). *Environ Geol.* 2003;43(7): 842–851.
- [9] Payton CC, Hansen MN. Gypsum karst in southwestern Utah: failure and reconstruction of Quail Creek Dike. *Rep Okla Geol Surv Circ.* 2003; 109:293–303.
- [10] Dreybrodt W, Romanov D, Gabrovsek F. Karstification below dam sites: a model of increasing leakage from reservoirs. *Environ Geol.* 2002;42(5):518–524.

- [11] Rothwell RG, Thomson J, Kahler G. Low-sea-level emplacement of a very large Late Pleistocene 'megaturbidite' in the western Mediterranean Sea. *Nature*. 1998;392(6674):377–380.
- [12] Sultan N, Cochonat P, Canals M, Cattaneo A, Dennielou B, Hafidason H, Laberg JS, Long D, Mienert J, Trincardi F, Urgeles R, Vorren TO, Wilson C. Triggering mechanisms of slope instability processes and sediment failures on continental margins: a geotechnical approach. *Mar Geol*. 2004;213(1–4):291–321.
- [13] Vogt PR, Jung WY. Holocene mass wasting on upper non-Polar continental slopes—due to post-Glacial ocean warming and hydrate dissociation? *Geophys Res Lett*. 2002;29(15):1–4.
- [14] Freij-Ayoub R, Tan C, Clennell B, Tohidi B, Yang JH. A wellbore stability model for hydrate bearing sediments. *J Pet Sci Eng*. 2007;57(1–2):209–220.
- [15] Watson MN, Boreham CJ, Tingate PR. Carbon dioxide and carbonate cements in the Otway Basin: Implications for geological storage of carbon dioxide. *APPEA J*. 2004;44:703–720.
- [16] Espinoza DN, Kim SH, Santamarina JC. CO₂ geological storage—Geotechnical implications. *KSCE J Civil Eng*. 2011;15(4):707–719.
- [17] Renard F, Gundersen E, Hellmann R, Collombet M, Le Guen Y. Numerical modeling of the effect of carbon dioxide sequestration on the rate of pressure solution creep in limestone: Preliminary results. *Oil Gas Sci Technol-Rev L Inst Fr Pet*. 2005;60(2):381–399.
- [18] He WW, Hajash A, Sparks D. Creep compaction of quartz aggregates: Effects of pore-fluid flow—A combined experimental and theoretical study. *Am J Sci*. 2003;303(2):73–93.
- [19] Le Guen Y, Renard F, Hellmann R, Brosse E, Collombet M, Tisserand D, Gratier JP. Enhanced deformation of limestone and sandstone in the presence of high P_{CO2} fluids. *J Geophys Res-Solid Earth*. 2007;112(B5):1–21.
- [20] Kvamme B, Liu S. Reactive transport of CO₂ in saline aquifers with implicit geomechanical analysis. *Energy Procedia*. 2009;1(1):3267–3274.
- [21] Taron J, Elsworth D. Thermal-hydrologic-mechanical-chemical processes in the evolution of engineered geothermal reservoirs. *Int J Rock Mech Min Sci*. 2009;46(5):855–864.
- [22] Ledesert B, Hebert R, Genter A, Bartier D, Clauer N, Grall C. Fractures, hydrothermal alterations and permeability in the Soultz Enhanced Geothermal System. *C R Geosci*. 2010;342(7–8):607–615.
- [23] Okochi H, Kameda H, Hasegawa S-I, Saito N, Kubota K, Igawa M. Deterioration of concrete structures by acid deposition—an assessment of the role of rainwater on deterioration by laboratory and field exposure experiments using mortar specimens. *Atmos Environ*. 2000;34(18):2937–2945.
- [24] Xie S, Qi L, Zhou D. Investigation of the effects of acid rain on the deterioration of cement concrete using accelerated tests established in laboratory. *Atmos Environ*. 2004;38(27):4457–4466.
- [25] Marcus R, Feldman D, Nelson D, Rosen CJ, eds. *Fundamentals of Osteoporosis*. Burlington: Elsevier; 2009.
- [26] Fredd CN, Fogler HS. Influence of transport and reaction on wormhole formation in porous media. *AIChE J*. 1998;44(9):1933–1949.
- [27] Golfier F, Zarcone C, Bazin B, Lenormand R, Lasseux D, Quintard M. On the ability of a Darcy-scale model to capture wormhole formation during the dissolution of a porous medium. *J Fluid Mech*. 2002;457:213–254.
- [28] Hoefner ML, Fogler HS. Pore evolution and channel formation during flow and reaction in porous media. *AIChE J*. 1988;34(1):45–54.
- [29] Luo H, Quintard M, Debenest G, Laouafa F. Properties of a diffuse interface model based on a porous medium theory for solid-liquid dissolution problems. *Comput Geosci*. 2012;16(4):913–932.
- [30] Oltéan C, Golfier F, Buès MA. Numerical and experimental investigation of buoyancy-driven dissolution in vertical fracture. *J Geophys Res Solid Earth*. 2013;118(5):2038–2048.
- [31] Cha M, Santamarina JC. Dissolution of randomly distributed soluble grains: Post dissolution k₀-loading and shear. *Geotechnique*. 2014; <http://dx.doi.org/10.1680/geot.14-P-115>.
- [32] Tran MK, Shin H, Byun Y-H, Lee J-S. Mineral dissolution effects on mechanical strength. *Eng Geol*. 2012;125:26–34.
- [33] Truong QH, Eom YH, Lee JS. Stiffness characteristics of soluble mixtures. *Geotechnique*. 2010;60(4):293–297.
- [34] Muir Wood D, Maeda K, Nukudani E. Modelling mechanical consequences of erosion. *Geotechnique*. 2010;60:447–457.
- [35] Shin H, Santamarina JC, Cartwright JA. Contraction-driven shear failure in compacting uncemented sediments. *Geology*. 2008;36(12):931–934.
- [36] Fam MA, Cascante G, Dusseault MB. Large and small strain properties of sands subjected to local void increase. *J Geotech Geoenviron Eng*. 2002;128(12):1018–1025.
- [37] Shin H, Santamarina JC. Mineral dissolution and the evolution of k₀. *J Geotech Geoenviron Eng*. 2009;135(8):1141–1147.
- [38] Lee JS, Tran MK, Lee C. Evolution of layered physical properties in soluble mixture: Experimental and numerical approaches. *Eng Geol*. 2012;143:37–42.
- [39] McDougall J, Kelly D, Barreto D. Particle loss and volume change on dissolution: experimental results and analysis of particle size and amount effects. *Acta Geotech*. 2013;8(6):619–627.
- [40] Zheng B, Elsworth D. Evolution of permeability in heterogeneous granular aggregates during chemical compaction: Granular mechanics models. *J Geophys Res Solid Earth*. 2012;117(B3):B03206.
- [41] Hu LB, Hueckel T. Coupled chemo-mechanics of intergranular contact: Toward a three-scale model. *Comput Geotech*. 2007;34(4):306–327.
- [42] Pietruszczak S, Lydzba D, Shao JF. Modelling of deformation response and chemo-mechanical coupling in chalk. *Int J Numer Anal Methods Geomech*. 2006;30(10):997–1018.
- [43] Cundall PA, Strack ODL. Discrete numerical-model for granular assemblies. *Geotechnique*. 1979;29(1):47–65.
- [44] Bagi K. An algorithm to generate random dense arrangements for discrete element simulations of granular assemblies. *Granular Matter*. 2005;7(1):31–43.
- [45] O'sullivan C. *Particulate Discrete Element Modelling: A Geomechanics Perspective*. New York: Taylor & Francis; 2011.
- [46] Cha M. *Mineral dissolution in sediments* (Ph.D. thesis), Atlanta, GA USA: Georgia Institute of Technology; 2012.
- [47] Cha M, Santamarina J, Kim H, Cho G. Small-strain stiffness, shear-wave velocity, and soil compressibility. *J Geotech Geoenviron Eng*. 2014;06014011 [http://dx.doi.org/10.1061/\(ASCE\)GT.1943-5606.0001157](http://dx.doi.org/10.1061/(ASCE)GT.1943-5606.0001157).
- [48] Jang J, Narsilio GA, Santamarina JC. Hydraulic conductivity in spatially varying media—a pore-scale investigation. *Geophys J Int*. 2011;184(3):1167–1179.
- [49] Cohen CE, Ding D, Quintard M, Bazin B. From pore scale to wellbore scale: Impact of geometry on wormhole growth in carbonate acidization. *Chem Eng Sci*. 2008;63(12):3088–3099.
- [50] Buijse MA. Understanding wormholing mechanisms can improve acid treatments in carbonate formations. *SPE Prod Facil*. 2000;15(3):168–175.